Journal of Controlled Release 314 (2019) 1–11

Contents lists available at ScienceDirect

Journal of Controlled Release

journal homepage: www.elsevier.com/locate/jconrel

Stromal-targeting radioimmunotherapy mitigates the progression of therapy-resistant tumors

Evangelia Bolli[a,b,1], Matthias D'Huyvetter[c,1], Aleksandar Murgaski[a,b], Danielle Berus[d], Geert Stangé[e], Emile J. Clappaert[a,b], Sana Arnouk[a,b], Ana Rita Pombo Antunes[a,b], Ahmet Krasniqi[c], Tony Lahoutte[c], Amanda Gonçalves[f,g,h], Marnik Vuylsteke[i], Geert Raes[a,b], Nick Devoogdt[c,2], Kiavash Movahedi[a,b,2], Jo A. Van Ginderachter[a,b,*]

[a] Laboratory of Myeloid Cell Immunology, VIB Center for Inflammation Research, Brussels, Belgium
[b] Laboratory of Cellular and Molecular Immunology, Vrije Universiteit Brussel, Brussels, Belgium
[c] In vivo Cellular and Molecular Immunology Laboratory, Vrije Universiteit Brussel, Brussels, Belgium
[d] Department of Radiation Protection, Vrije Universiteit Brussel, UZ Brussel, Brussels, Belgium
[e] Diabetes Research Center, Vrije Universiteit Brussel, Brussels, Belgium
[f] VIB Center for Inflammation Research, Ghent, Belgium
[g] Department of Biomedical Molecular Biology, Ghent University, Ghent, Belgium
[h] VIB Bio Imaging Core Gent, Ghent, Belgium
[i] Gnomixx, Melle, Belgium

ARTICLE INFO

Keywords:
Tumor-associated macrophage
Hypoxia
Nanobody
Radioimmunotherapy
Immune checkpoint blockade

ABSTRACT

Radioimmunotherapy (RIT) aims to deliver a high radiation dose to cancer cells, while minimizing the exposure of normal cells. Typically, monoclonal antibodies are used to target the radionuclides to cancer cell surface antigens. However, antibodies face limitations due to their poor tumor penetration and suboptimal pharmacokinetics, while the expression of their target on the cancer cell surface may be gradually lost. In addition, most antigens are expressed in a limited number of tumor types. To circumvent these problems, we developed a Nanobody (Nb)-based RIT against a prominent stromal cell (stromal-targeting radioimmunotherapy or STRIT) present in nearly all tumors, the tumor-associated macrophage (TAM). Macrophage Mannose Receptor (MMR) functions as a stable molecular target on TAM residing in hypoxic areas, further allowing the delivery of a high radiation dose to the more radioresistant hypoxic tumor regions. Since MMR expression is not restricted to TAM, we first optimized a strategy to block extra-tumoral MMR to prevent therapy-induced toxicity. A 100-fold molar excess of unlabeled bivalent Nb largely blocks extra-tumoral binding of ^{177}Lu-labeled anti-MMR Nb and prevents toxicity, while still allowing the intra-tumoral binding of the monovalent Nb. Interestingly, three doses of ^{177}Lu-labeled anti-MMR Nb resulted in a significantly retarded tumor growth, thereby outcompeting the effects of anti-PD1, anti-VEGFR2, doxorubicin and paclitaxel in the TS/A mammary carcinoma model. Together, these data propose anti-MMR STRIT as a valid new approach for cancer treatment.

1. Introduction

Several treatment options against cancer, including chemotherapy and radiation therapy, often display a low therapeutic window due to the lack of specificity for cancer cells and the effect on normal cells with high mitotic rates. A possible solution to this problem is the targeted delivery of therapeutic payloads to the tumor microenvironment. In this respect, antibody-drug conjugates (ADC) take advantage of the

Abbreviations: ALT, alanine aminotransferase; ADC, antibody-drug conjugate; DAPI, 4′, 6-diamidino-2-phenylindole; HP, histopathological parameters; IA/g, injected activity per gram tissue; IMRT, Intensity Modulated Radiation Therapy; MAR, micro-autoradiography; MMR, macrophage mannose receptor; Nb, nanobody; PFA, paraformaldehyde; p.i, post-injection; RIT, radioimmunotherapy; REML, residual maximum likelihood; STRIT, stromal-targeting radioimmunotherapy; TRNT, targeted radionuclide therapy; TAM, tumor-associated macrophage

* Corresponding author at: Lab of Cellular and Molecular Immunology, VIB-Vrije Universiteit Brussel, Building E8, Pleinlaan 2, B-1050 Brussels, Belgium.
E-mail address: jo.van.ginderachter@vub.be (J.A. Van Ginderachter).

[1] Shared first authorship
[2] Shared senior authorship

https://doi.org/10.1016/j.jconrel.2019.10.024
Received 4 January 2019; Received in revised form 17 September 2019; Accepted 12 October 2019
Available online 15 October 2019
0168-3659/

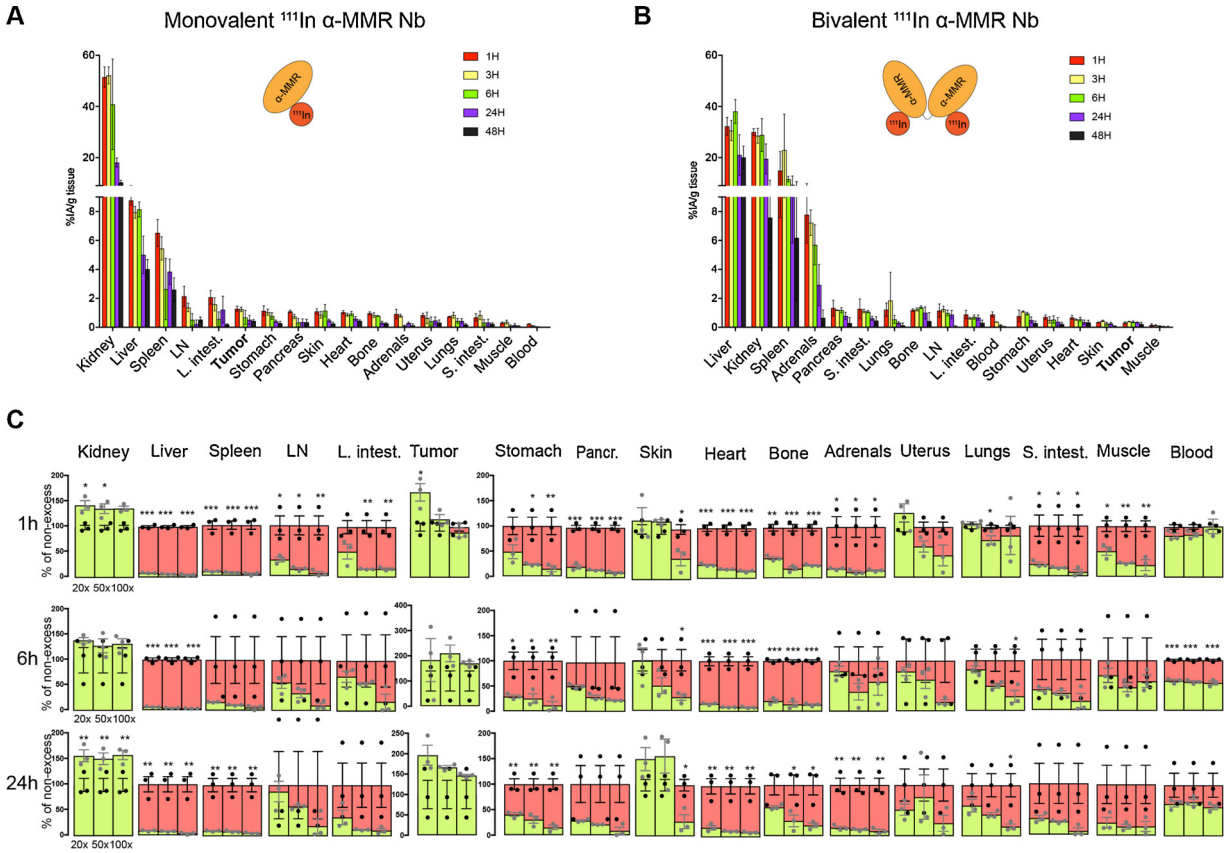

Fig. 1. In vivo biodistribution of differently formulated α-MMR Nbs. Biodistribution of **A)** ^{111}In-DTPA- monovalent α-MMR Nb and **B)** ^{111}In-DTPA- bivalent α-MMR Nb at different time points (1 h, 3 h, 6 h, 24 h and 48 h). n = 3 mice per time point. **C)** Biodistribution of ^{111}In-DTPA monovalent α-MMR Nb co-injected with a 20-, 50- or 100-fold molar excess of unlabeled bivalent α-MMR Nb. Organs/Tissues were dissected at 1 h, 6 h and 24 h p.i. and tracer uptake in tissues was plotted as % of the uptake in mice that did not receive the excess of unlabeled bivalent α-MMR Nb (green bars). Red bars indicate the % reduced uptake between the condition without excess (= 100%) and the condition with excess. n = 3 mice per different fold excess of unlabeled bivalent α-MMR Nb. Tracer uptake was expressed as %IA/g of tissue. Statistical analysis was performed between no excess group and different excesses using Students' *t*-test, $p \leq 0.05$.

exquisite specificity of antibodies to deliver a therapeutic compound to the target cells *in vivo*, with a minimal exposure of healthy tissues during treatment. [1] A variant of this approach is the coupling of radiotherapeutic isotopes to antibodies for targeted radionuclide therapy (TRNT) or radioimmunotherapy (RIT), delivering high radiation doses to the target cells [2]. Up to now, only cancer cells were reported as RIT targets, with a radiolabeled α-CD20 mAb (^{90}Y-Ibritumomab tiuxetan; Zevalin) being the only marketed product so far. [3] Likewise, more than 65 ADCs are in different phases of clinical trials against a variety of cancer types, all of which are targeting a cancer cell marker [1].

Notably, the *in vivo* pharmacokinetic properties of conventional antibodies may challenge the success of RIT, especially in the case of solid tumors. Single-domain antibody fragments, also termed Nanobodies (Nbs), derived from Camelidae heavy-chain-only antibodies were shown to be favorable over monoclonal antibodies or other antibody-derived fragments due to their small size (10–15 kDa) that permits deep penetration into tissues (including tumors) and fast blood clearance, high stability, affinity and solubility. [4] The efficacy of Nb-mediated radioimmunotherapy against CD20, Her-2 and the multiple myeloma idiotype, has been demonstrated in preclinical cancer models [5–7].

However, potential caveats of targeting cancer cell markers are the restricted expression of these markers on particular cancer types and the loss of the marker on mutated cancer cells. A solution to this problem could be the targeting of non-transformed tumor-associated cells that stably express the molecular target. Tumor-associated macrophages (TAMs) are among the most abundant tumor-infiltrating leukocytes and are related to poor prognosis in the majority of cancer types. [8] We previously reported that TAMs residing in hypoxic areas express high levels of the Macrophage Mannose Receptor (MMR, CD206) and can be specifically targeted by α-MMR Nbs [9–11].

Hypoxia is detrimental for radiation therapy since it mediates increased cancer cell radioresistance, implying that the most hypoxic regions require higher radiation doses. [12] Here, we propose RIT targeted to a stromal cell (stromal-targeting radioimmunotherapy or STRIT) as a therapeutic option, whereby hypoxic MMR^{high} TAMs were targeted with a ^{177}Lu-labeled MMR-specific Nb. This approach delivered a high radiation dose to the radioresistant hypoxic regions and significantly impaired the progression of tumors that were otherwise resistant to conventional therapies. Hence, α-MMR Nbs have a strong potential, not only as a tool for molecular imaging [11] but also for cancer therapy.

2. Results

2.1. Biodistribution of ^{111}In-labeled α-MMR Nbs and optimal blocking strategy to prevent potential therapy-induced toxicity

To assess the possibility of α-MMR Nb-mediated STRIT, we employed the TS/A mammary adenocarcinoma model grown s.c. in Balb/c mice. We previously reported the accumulation of ^{99m}Tc-labeled α-MMR Nb in hypoxic areas of this tumor, binding to MMR^{high} macrophages in these sites. [10] Importantly, co-injection of a 20-fold molar excess of unlabeled bivalent Nb could block most of the extra-tumoral binding sites of the ^{99m}Tc-labeled monovalent Nb, due to the higher

avidity and lower tumor penetrance of the bivalent Nb, allowing its accumulation in the tumor for imaging purposes (within a timeframe of 3 h). [10] However, a therapeutic approach such as STRIT requires a more prolonged blockade of extra-tumoral binding sites, creating the risk that non-radioactively labeled bivalent α-MMR Nb could also accumulate in the tumor in the course of time, diminishing the efficacy of RIT with radioactively labeled monovalent α-MMR Nb. Hence, the biodistribution of both monovalent and bivalent ^{111}In-labeled α-MMR Nb was evaluated over a 48 h time window. ^{111}In is a γ-emitter widely used in diagnostic studies due to its half-life of 2.8 days. TS/A tumor-bearing mice (13 days s.c. tumor growth) were intravenously injected with ^{111}In-DTPA- monovalent α-MMR Nb (1.30 ± 0.08 MBq/2 μg Nb, RCP: 97.3%) (Fig. 1A, **S1A, Table S2 top panel**) or ^{111}In-DTPA- bivalent α-MMR Nb (0.53 ± 0.05 MBq/1 μg bivalent Nb, RCP: 96.7%) (Fig. 1B, **S1B, Table S2 bottom panel**) and biodistribution was evaluated by γ-counting of tissue dissected at 1 h, 3 h, 6 h, 24 h and 48 h post-injection (p.i.). Uptake of ^{111}In-labeled monovalent α-MMR Nb, expressed as injected activity per gram tissue (%IA/g), was already detected at 1 h p.i. in the tumor and extra-tumoral sites like liver and spleen with uptake values of 1.28 ± 0.18, 8.76 ± 0.31 and 6.52 ± 0.93%IA/g, respectively. This uptake gradually declined at later time points, reaching values of 0.45 ± 0.09, 4.02 ± 0.67 and 2.6 ± 0.81%IA/g at 48 h p.i. for tumor, liver and spleen, respectively. On the other hand, ^{111}In-labeled bivalent α-MMR Nb was detected at very high amounts in the extra-tumoral sites at 1 h p.i. (32.23 ± 3.46 and 14.93 ± 7.36%IA/g for liver and spleen, respectively), while tumor uptake was negligible with only 0.32 ± 0.07%IA/g. Importantly, the gradually declining uptake of the bivalent Nb in extra-tumoral sites at later time points (20.08 ± 4.4 and 6.18 ± 4.36%IA/g at 48 h p.i. for liver and spleen, respectively), is not accompanied by an increase in tumor uptake (remains very low at 0.23 ± 0.13%IA/g at 48 h p.i.), illustrating the lack of intra-tumoral accumulation of the bivalent construct. This implies that an excess of unlabeled bivalent α-MMR Nb is not expected to prevent tumor uptake of the therapeutic monovalent α-MMR Nb when co-administered in a multiple-dose treatment regimen.

To fully prevent STRIT-mediated organ toxicity, the uptake of radiolabeled monovalent α-MMR Nb in extra-tumoral tissues needs to be minimized. Therefore, we set out to optimize the blocking strategy and assessed the ability of increasing amounts of excess unlabeled bivalent α-MMR Nb to block extratumoral binding of the monovalent α-MMR Nb, while maintaining its high tumor targeting. Hence, ^{111}In-labeled monovalent α-MMR Nb (2.05 ± 0.17 MBq/1 μg Nb; RCP: 96%) was injected concomitantly with a 20-, 50- and 100-fold molar excess of unlabeled bivalent α-MMR Nb in TS/A tumor-bearing mice and its biodistribution was evaluated at 1 h, 6 h and 24 h p.i. At all time-points examined, co-injection of unlabeled bivalent excess enhanced ^{111}In-labeled monovalent α-MMR Nb tumor targeting, while probe uptake in other organs was significantly reduced (Fig. 1C, **Tables S3-5**). In this regard, a 100-fold bivalent excess most efficiently reduced extra-tumoral uptake of monovalent Nb to very low levels, while tumor uptake remained high (Fig. 1C), constituting a valid approach to prevent undesirable extra-tumoral targeting.

2.2. Biodistribution of ^{111}In-DTPA-monovalent α-MMR Nb as determined via molecular imaging

To visualize the distribution of the radioactively labeled monovalent α-MMR Nb within the tumor (with and without blocking with an excess of unlabeled bivalent α-MMR Nb), micro-SPECT/CT images in 13-days s.c. TS/A tumor-bearing mice were generated and quantified (Fig. 2, **Table S6**) after i.v. injection of ^{111}In-DTPA-monovalent non-targeting R3B23 Nb (10.78 ± 0.13 MBq/2 μg Nb; RCP: 99.4%) and ^{111}In-DTPA-monovalent α-MMR Nb alone (18.75 ± 0.83 MBq/3 μg Nb; RCP: 99%), or with a 50-fold molar excess of unlabeled bivalent α-MMR Nb. All samples were co-injected with 150 mg/kg gelofusine to reduce the amount of radioactivity retained in kidneys [13]. High contrast images were obtained as early as 1 h p.i., with most radioactivity concentrated in kidneys, liver and tumor in the case of a single ^{111}In-DTPA-monovalent α-MMR Nb injection. As expected, ^{111}In-DTPA-monovalent non-targeting R3B23 Nb only showed radioactivity in kidney and bladder. Co-injection with a 50-fold molar excess of unlabeled bivalent α-MMR Nb prevented the uptake of ^{111}In-DTPA-monovalent α-MMR Nb in liver and other organs without dramatically reducing tumor targeting, which is in line with the data obtained by *ex vivo* dissections (Fig. 1C, **Table S3**).

2.3. Biodistribution of therapeutic ^{177}Lu-DTPA-monovalent α-MMR Nb

Having optimized the in vivo procedure for optimal tumor targeting of the monovalent anti-MMR Nb, we next turned to the use of therapeutic ^{177}Lu-labeled anti-MMR Nb. In first instance, we examined the biodistribution of the therapeutic regimen in 13-day-old s.c. TS/A tumors via serial dissections (Fig. 3, **Table S7**). The highest tumor uptake for ^{177}Lu-DTPA-monovalent α-MMR Nb (8.63 ± 0.24 MBq/1.5 μg Nb; RCP: 99.4%), co-injected simultaneously with a 100-fold molar excess of unlabeled bivalent α-MMR Nb and 150 mg/kg gelofusine, was observed after 1 h, with a value of 1.30 ± 0.21%IA/g, and decreased to 0.56 ± 0.09%IA/g at 24 h and to 0.27 ± 0.02%IA/g at 72 h. In kidneys, 11.92 ± 1.25 % IA/g was measured at 1 h, decreasing rapidly to 4.09 ± 0.84 % IA/g at 24 h and to 1.61 ± 0.07 % IA/g at 72 h. Uptake in other organs was negligible. Importantly, bone uptake was very low at all time points, indicating that no substantial loss of free ^{177}Lu (indicative of degradation of the therapeutic compound) occurred. In mice bearing TS/A tumors orthotopically growing in the mammary fat pad, the biodistribution data of ^{177}Lu-DTPA-monovalent α-MMR Nb (6.46 ± 0.29 MBq/1.5 μg Nb, RCP: 98.8%) were largely similar (**Figure S2**, **Table S8**), indicating that α-MMR STRIT could also be applicable to deeper growing tumors.

2.4. Excess of bivalent α-MMR Nb protects against therapy-induced toxicity

A major concern for the *in vivo* application of ^{177}Lu-labeled monovalent anti-MMR Nb is therapy-induced organ toxicity, which, based on our biodistribution data (Fig. 1,2), should be minimized by a 100-fold molar excess of bivalent anti-MMR Nb. To prove this point, we injected a 100-fold molar excess of unlabeled bivalent α-MMR Nb concomitantly with a single high dose (48.21 ± 2.64 MBq/1.7 μg Nb; RCP:95.2%) of therapeutic ^{177}Lu-labeled α-MMR Nb in naive animals. While the mortality rate reached 83,3% within 24 days when mice received ^{177}Lu-labeled α-MMR Nb alone, all mice survived for at least 35 days upon co-injecting a 100-fold excess of bivalent Nb (Fig. 4A). These results demonstrate the clear benefit of blocking extra-tumoral binding sites with a high excess of bivalent α-MMR Nb in a therapeutic context.

We then switched to a more therapeutically relevant regimen of 3 consecutive injections of a lower dose of ^{177}Lu-labeled α-MMR Nb (25.91 ± 6.38 MBq/1.5 μg Nb; RCP > 95%) in naive mice with or without 100-fold bivalent excess and analyzed the long-term survival and signs of pathology (Fig. 4B). These mice also received 150 mg/kg gelofusine, to reduce the retention of therapeutic radioactivity in kidney tubular cells. [13] In this setup, all mice survived, irrespective of the blocking strategy. However, without blockade, tubulopathy was observed in the treated mice after about 100 days and consisted of an increased incidence of mostly tubular degeneration (indicated by circles and characterized by epithelial shrinkage and tubular dilation) and to a lesser extent of thickened basal laminae and single cases of karyomegaly (indicated by arrowheads) or interstitial focal fibrosis. Importantly, there were no such lesions in the group co-injected with the 100-fold bivalent excess or the control group receiving 0.9% saline, further highlighting the protective advantage of the blocking strategy (Fig. 4B, Table 1A). No specific lesions were observed in liver nor spleen (being the organs with the highest uptake of α-MMR Nb in the absence

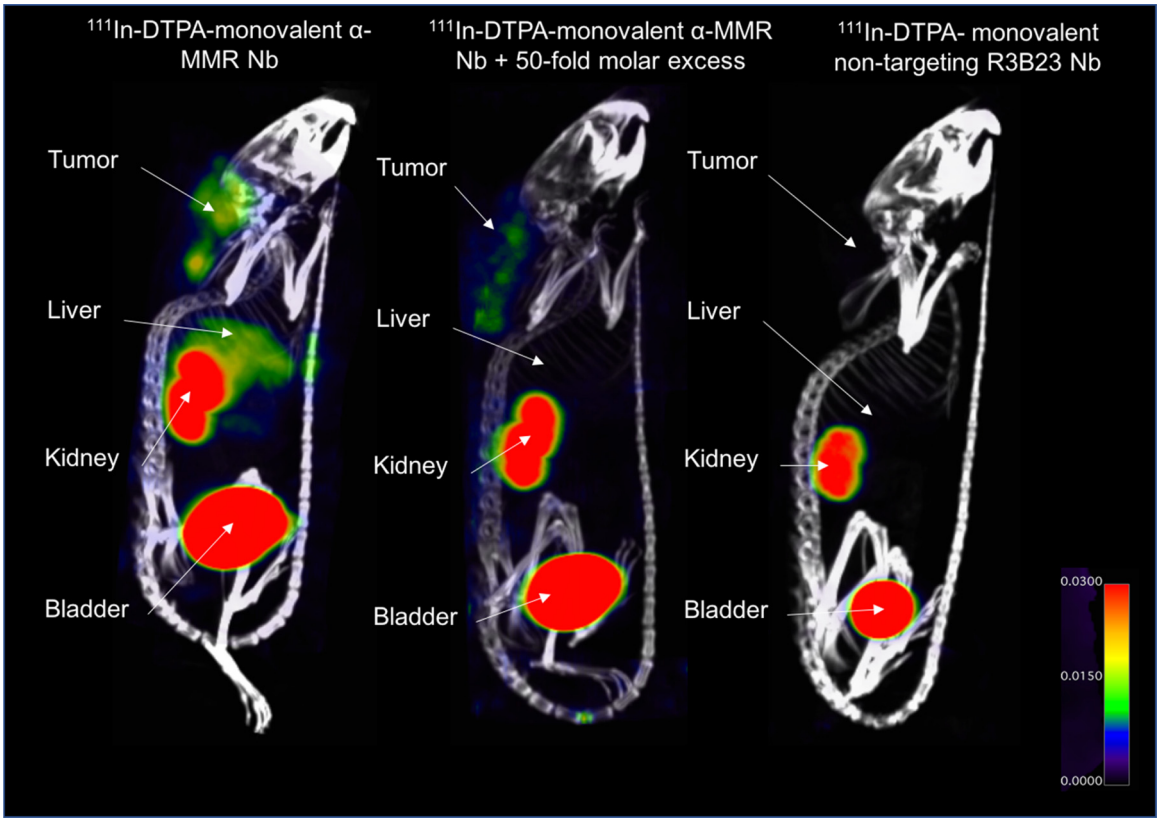

Fig. 2. Micro-SPECT/CT images of ^{111}In-DTPA-monovalent α-MMR Nb. Micro-SPECT/CT images were obtained in the TS/A tumor model at 1 h after injection of either ^{111}In-DTPA-monovalent non-targeting R3B23 Nb or ^{111}In-DTPA-monovalent α-MMR Nb alone, or with a 50-fold molar excess of unlabeled bivalent α-MMR Nb. Accumulation of radioactivity was observed in kidneys, liver, bladder and tumor, indicated by white arrows.

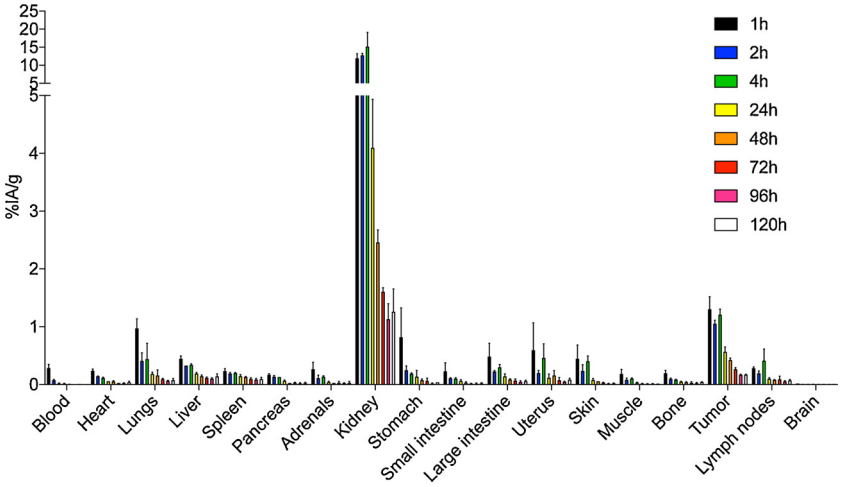

Fig. 3. In vivo biodistribution of ^{177}Lu-DTPA-monovalent α-MMR Nbs. Ex vivo biodistribution of ^{177}Lu-DTPA-monovalent α-MMR Nb, co-injected with a 100-fold molar excess of unlabeled bivalent α-MMR Nb and 150 mg/kg gelofusine, at several time points up to 120 h in mice with TS/A tumors (% IA/g). Data are presented as mean ± SD (n = 3).

of blockade) (data not shown) and ALT levels in the serum, indicative of liver toxicity, were not elevated (Table 1A).

Finally, to assess for toxicity in a cancer therapy setting, 3 and 6 injections of monovalent ^{177}Lu-labeled α-MMR Nb (25.91 ± 6.38 MBq/1.5 μg Nb; RCP > 95%) or 0.9% saline were administered to TS/A tumor-bearing mice (Fig. 4C). Every therapeutic shot was accompanied by the simultaneous co-injection of a 100-fold excess of bivalent Nb and 150 mg/kg gelofusine for kidney protection. The organ-absorbed doses for a cumulative administration of 26, 78 and 156 MBq (corresponding to the described 1, 3 and 6 dose-regimens) of ^{177}Lu-DTPA-monovalent α-MMR Nb with a 100-fold molar excess of unlabeled bivalent α-MMR Nb and 150 mg/kg gelofusine, are summarized in Table 2. The highest absorbed dose was delivered to kidneys (9.20, 27.60 and 55.21 Gy for 26, 78 and 156 MBq respectively), while tumors received 1.11, 3.32 and 6.64 Gy for 26, 78 and 156 MBq respectively. Doses delivered

to other healthy organs and tissues were low. Histopathological analysis revealed that mostly animals receiving the 6-dose treatment (Fig. 4C3), but not the saline-treated group (Fig. 4C1) and to a lesser extent the 3-dose treatment (Fig. 4C2), developed a moderate tubulopathy that was characterized by hyaline casts within the relatively short time frame of the experiment (25 days) (Table 1B). No lesions were observed in liver and spleen via histopathological analysis (data not shown) and ALT levels in the serum were not elevated (Table 1B). Collectively, these findings demonstrate the importance of excess bivalent α-MMR Nb in the protection against therapy-induced toxicity

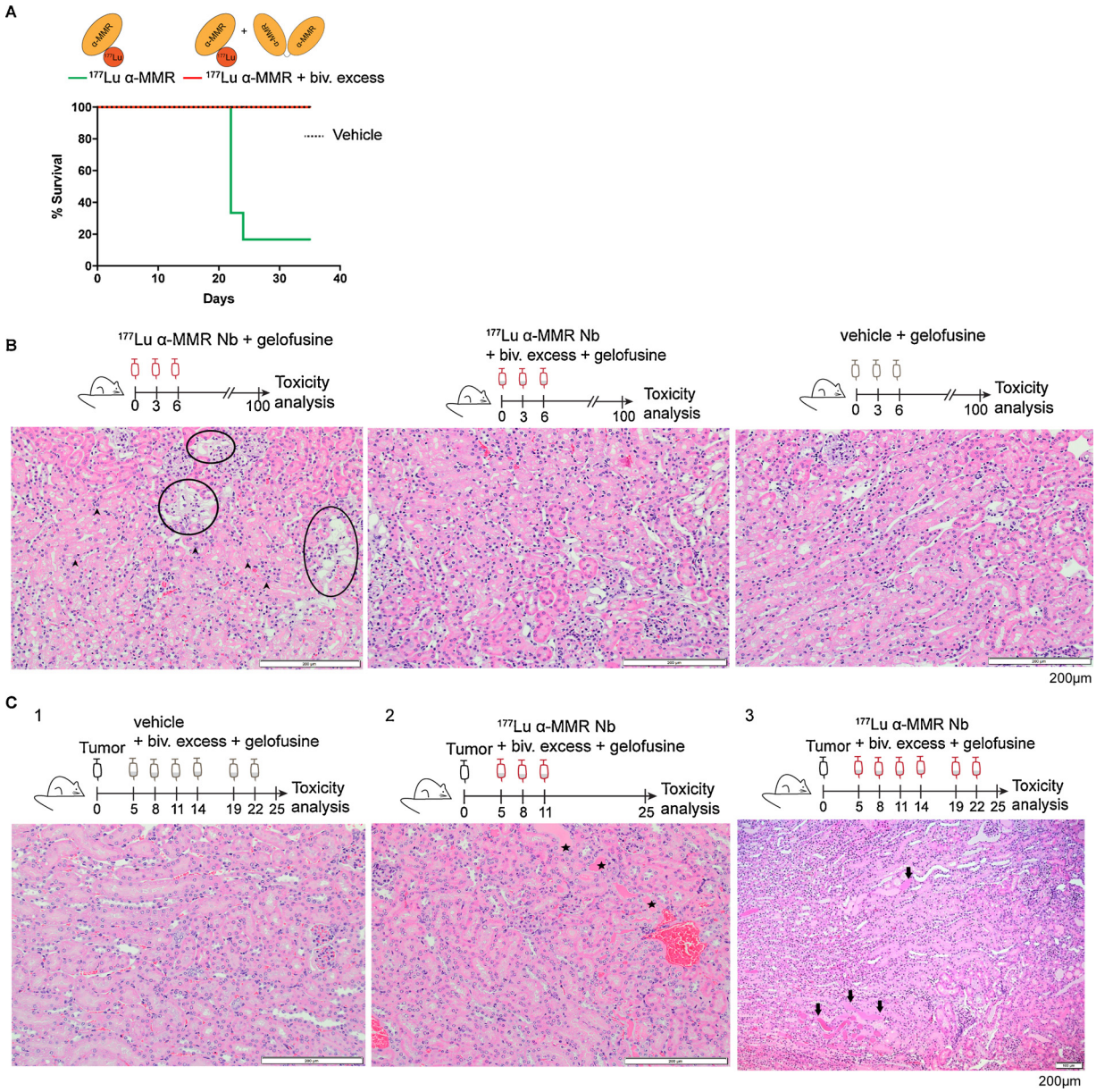

Fig. 4. Prevention of systemic toxicity by ^{177}Lu-labeled α-MMR Nb. A) Survival curve of naïve Balb/c mice that received a single dose of ^{177}Lu-labeled α-MMR Nb with or without the blocking strategy (simultaneous co-injection, n = 6). B) Naïve Balb/c mice received 3 doses of ^{177}Lu-labeled α-MMR Nb with or without the blocking strategy and gelofusine (simultaneous co-injection, n = 5). All mice survived until about 100 days, when the mice were sacrificed and the kidneys were isolated for histopathological analysis (n = 3). Circles indicate tubular degeneration and arrowheads indicate karyomegaly. C1) Histopathological analysis of kidneys of TS/A-bearing mice at day 25 of tumor growth, treated with 0.9% saline with 5 mg/ml ascorbic acid (vehicle) or C2) 3 dose regimens of ^{177}Lu-labeled α-MMR Nb (asterisks indicate hyaline tubular casts) or C3) 6 dose regimens of ^{177}Lu-labeled α-MMR Nb (arrows indicate hyaline tubular casts). (n = 3).

with the kidneys being the dose-limiting organ of the therapeutic radiolabeled α-MMR Nb.

2.5. Stromal-targeting radioimmunotherapy inhibits the growth of therapy-resistant tumors

Next, we determined the therapeutic efficacy of α-MMR Nb-mediated STRIT using the treatment regimens as described in Fig. 4C. Interestingly, multiple-dose treatments (3 or 6 injections) with ^{177}Lu-labeled α-MMR Nb (25.91 ± 6.38 MBq/1.5 µg Nb; RCP > 95%) resulted in a significantly delayed TS/A tumor growth as compared to the single dose or saline-treated groups (Fig. 5A). 3 doses of an irrelevant ^{177}Lu-labeled non-targeting Nb (R3B23, 25.91 ± 6.38 MBq/1.5 µg Nb; RCP > 95%) did not cause reduced tumor growth as compared to the saline-treated group (Fig. 5B). As a final control, unlabeled monovalent α-MMR Nb (= vehicle) had no effect on tumor growth either (Fig. 5C). All treated mice received a 100-fold excess of bivalent α-MMR Nb and 150 mg/kg gelofusine, as described before. Since the 6 and 3-dose regimens showed comparable therapeutic efficacy, the latter was considered for further investigation due to the higher toxicity that was observed for the 6-dose regimen (Table 1B).

Based on our previously published data [10], the anti-tumor effect of STRIT is expected to at least partly result from anti-MMR Nb accumulation in hypoxic tumor areas. In order to visualize STRIT accumulation in the tumor, a 3-dose regimen of ^{177}Lu-labeled α-MMR Nb (25.91 ± 6.38 MBq/1.5 µg Nb; RCP > 95%) was administered to TS/A tumor bearing mice, following the same schedule as illustrated in Fig. 4C2, after which micro-autoradiography (Fig. 6**A1**) and immunohistology for hypoxia and MMR (Fig. 6A2-4) were performed on histological slides of 12-day-old tumors (i.e. 1 day after the last

Table 1
Toxicity in liver and kidneys of A) naïve Balb/c and B) TS/A tumor-bearing mice treated with ^{177}Lu-labeled α-MMR Nb as described in Figs. 4B and 4C. Histopathological parameters (HP) were measured (Supplementary Material and Methods, n = 3). Liver functionality was also examined by measuring the activity of Alanine Aminotransferase (ALT, mU/ml) in the serum. Values are Mean ± SD (n = 5–6). For kidney histopathology the following parameters were tested: tubular casts, hyaline (TC, H), thickened basal laminae (TBL), karyomegaly (K), tubular degeneration (TD), fibrosis- interstitial (F) and other histopathology (other HP: mononuclear foci, fibrosis- suburothelial). HP; histopathology, N.d; non detectable, x/y; number of affected mice/mean severity. y value of 1 < 2 < 3 corresponds to minimal < slight < moderate grade of severity.

	Liver ALT (mU/ml)		Kidney HP					
	Mean	SD	TC, H	TBL	K	TD	F	Other HP
A								
3x saline + gelofusine	11,1	7,6	N.d	N.d	N.d	N.d	N.d	N.d
3x ^{177}Lu α-MMR Nb + gelofusine	12,3	3,6	N.d	3/1.0	1/1.0	3/2.0	1/1.0	N.d
3x ^{177}Lu α-MMR Nb + biv. excess + gelofusine	15,5	8,6	N.d	N.d	N.d	N.d	N.d	N.d
B								
6x saline + biv. Excess + gelofusine	5,9	4,0	N.d	N.d	N.d	N.d	N.d	N.d
3x ^{177}Lu α-MMR Nb + biv. excess + gelofusine	5,1	0,6	1/2.0	N.d	N.d	N.d	N.d	N.d
6x ^{177}Lu α-MMR Nb + biv. excess + gelofusine	5,0	0,6	3/3.0	N.d	N.d	N.d	N.d	N.d

Table 2
Dosimetry analysis. Radiation doses from a cumulative administration of 26, 78 and 156 MBq (corresponding to the described 1, 3 and 6 dose-regimens) of ^{177}Lu-DTPA-monovalent α-MMR Nb with a 100-fold molar excess of unlabeled bivalent α-MMR Nb and 150 mg/kg gelofusine were calculated using trapezoid integration of measured radionuclide activity in tissues of interest and expressed in Gy.

Organ/tissue	Gy		
	26 MBq	78 MBq	156 MBq
Lung	0,39	1,18	2,35
Heart	0,13	0,40	0,80
Liver	0,42	1,25	2,51
Kidney	**9,20**	**27,60**	**55,21**
Spleen	0,31	0,94	1,88
Muscle	0,07	0,20	0,40
Bone	0,11	0,34	0,68
Blood	0,02	0,07	0,13
Tumor	**1,11**	**3,32**	**6,64**

treatment). Within STRIT-treated tumors, the ^{177}Lu tracer accumulated mainly in the hypoxic tumor areas co-localized with MMR expression as determined via micro-autoradiography (Fig. 6A1-4). Areas with radionuclide deposition were not present in the control groups which were treated with non-targeting ^{177}Lu-labeled R3B23 Nb (25.91 ± 6.38 MBq/1.5 μg Nb; RCP > 95%), saline or unlabeled α-MMR Nb (data not shown), proving further the specificity of STRIT therapy that is attributed to MMR-driven accumulation of the radioactive tracer in the tumor.

Notably, when staining for the apoptosis-indicator cleaved caspase-3 at this 12-day time point, apoptotic cells were mainly observed within the hypoxic, macrophage-rich areas of tumors (**Figure S3A1-4**). An automated quantification of cleaved caspase-3$^+$ cells indicated a higher presence of apoptotic cells in tumors from ^{177}Lu-α-MMR Nb-treated mice as compared to tumors from non-targeting ^{177}Lu-labeled R3B23 Nb-treated mice or unlabeled anti-MMR Nb-treated mice (**Figure S3B**).

Finally, we looked at the end stage of the experiment at day 25 (i.e. two weeks after the last treatment) to assess whether α-MMR Nb-mediated STRIT had a long-lasting effect on the tumor immune compartment. F4/80$^+$MMR$^+$ macrophages, B220$^+$ B cells, CD4$^+$ T cells and CD8$^+$ T cells from TS/A tumors were quantified via immunohistology in treated (3 or 6 doses) and control tumors (Fig. 7A). No significant changes were observed in the density of these immune cells within late stage tumors of ^{177}Lu-anti-MMR Nb-treated mice (Fig. 7B), suggesting that the therapeutic effect of STRIT did not rely on long-term macrophage depletion or an increased lymphocyte influx.

2.6. MMR-targeted STRIT outcompetes the efficacy of currently used therapies

We next examined how α-MMR STRIT compares to currently used therapies, including immune checkpoint blockade (α-PD1), anti-angiogenic therapy (α-VEGFR2) and chemotherapy (doxorubicin, paclitaxel) in the TS/A breast carcinoma model. Furthermore, we wished to assess whether α-MMR Nb-mediated STRIT can work synergistically in a combination therapy. Different treatment regimens were assessed, as illustrated in Fig. 8, demonstrating the relative resistance of TS/A

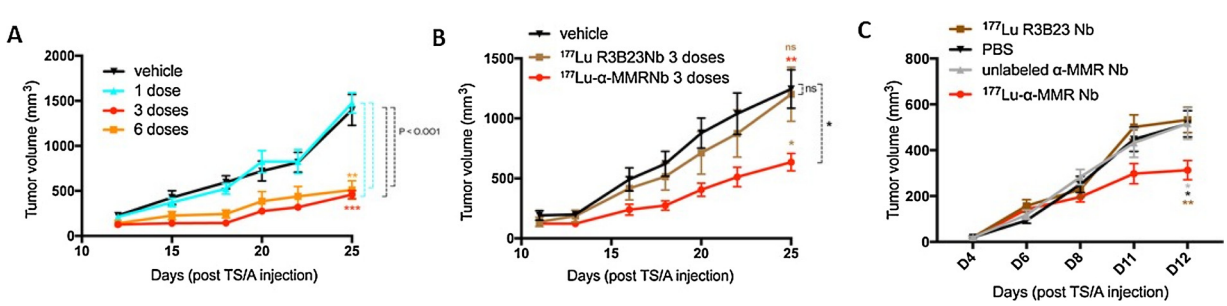

Fig. 5. MMR-targeted STRIT delays tumor growth. A) Tumor growth of TS/A-bearing mice treated with different regimens of ^{177}Lu-labeled α-MMR Nb. TS/A-bearing Balb/c mice were randomized into four groups (n = 6). Three groups received different dose regimens and the fourth group received 0.9% saline with 5 mg/ml ascorbic acid (vehicle) intravenously as a control, in addition to bivalent excess and gelofusine as indicated in Fig. 4C. B) Tumor growth of TS/A-bearing mice treated with ^{177}Lu-labeled α-MMR Nb or a control ^{177}Lu-labeled Nb (R3B23) in a 3-dose regimen (n = 7–8). C) Tumor growth of TS/A-bearing mice treated with ^{177}Lu-labeled α-MMR Nb, a control ^{177}Lu-labeled Nb (R3B23) or an unlabeled α-MMR Nb in a 3-dose regimen (n = 6). Tumor volume data were analyzed as repeated measurements (Genstat v19) and pairwise comparisons of the entire growth curves was done by a F-test; Student's *t*-test was performed to compare vehicle-treated mice to three and six dose regimens at day 25 of tumor growth. The statistical significance in the figures is indicated as follows: ns = not significant; *: $p < 0.05$; **: $p < 0.01$; ***: $p < 0.001$.

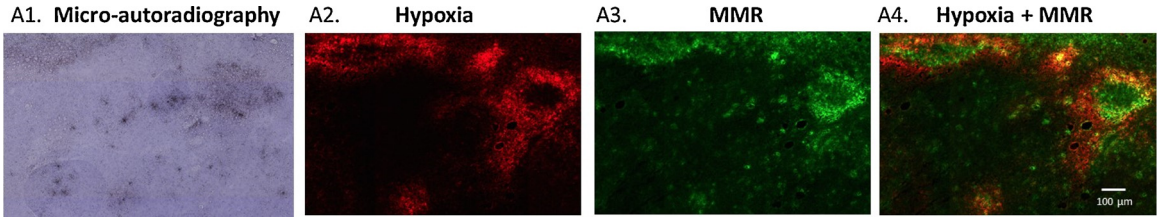

Fig. 6. ^{177}Lu-DTPA-anti-MMR Nb accumulates in hypoxic tumor areas that contain MMR^{high} cells. Consecutive slides of a 13-day-old TS/A tumor, treated with 3 doses of ^{177}Lu-DTPA-anti-MMR Nb, were either subjected to micro-autoradiography or stained with anti-MMR (green) or Hypoxyprobe (red; 2 h after in vivo pimonidazole injection).

tumors to a monotherapy with α-PD1 (Fig. 8A), α-VEGFR2 (Fig. 8B), a combination of α-PD1 and α-VEGFR2 (Fig. 8C) and monotherapy with doxorubicin or paclitaxel (Fig. 8D). Conversely, as a monotherapy, α-MMR STRIT provoked a significant anti-tumor effect, significantly outcompeting α-PD1, α-VEGFR2, doxorubicin and paclitaxel (Fig. 8A–D). This therapeutic efficacy of α-MMR STRIT was not significantly enhanced by a combination with any of these treatments. Together, these data identify α-MMR STRIT as an efficient therapeutic approach in tumors that are relatively resistant to immuno-, anti-angiogenic and chemotherapy.

3. Discussion

We provide a first proof-of-concept that an optimized protocol for radioimmunotherapy targeting MMR-expressing tumor-associated macrophages significantly reduces the growth of tumors that are relatively resistant to immune checkpoint blockade, anti-angiogenic therapy and chemotherapy. Resistance to standard-of-care treatments, such as chemotherapy, radiation and immunotherapy, is a major aspect of cancer dissemination, [14,15] which can be attributed to cancer cell-intrinsic genomic instability [16] and/or cancer cell-extrinsic factors such as hypoxia [17]. One approach to circumvent resistance is to deliver high doses of the therapeutic compound directly to the cancer cells. However, although targeted therapy seems to be advantageous at early stages of treatment, relapse always occurs due to the high tumor heterogeneity allowing the outgrowth of resistant cancer cell clones [18]. In this respect, our α-MMR STRIT aims to escape resistance by targeting the molecularly more stable population of TAMs that dominates the tumor milieu [19]. Interestingly, MMR^{high} TAMs depend on CSF1R signaling for their generation and maintenance [20] and reside mainly in the hypoxic tumor regions, where their phenotype becomes pro-tumoral under the influence of hypoxia. [21] The importance of hypoxia in determining the tumor-promoting activity of MMR^{high} TAMs is further proven by the diminished tumor growth in mice whose macrophages fail to migrate into hypoxic areas, due to a deficiency in the receptor Neuropilin-1. [22] Based on this knowledge, we developed α-MMR STRIT as a method to deliver a high radiation dose to the hypoxic regions, by targeting the stromal cells that reside there. We confirmed, via micro-autoradiography and immunohistology, that radioactively labeled anti-MMR Nb indeed accumulates in the hypoxic tumor regions where MMR^{hi} cells reside. Importantly, hypoxic regions are more radio-resistant, providing the rationale for Intensity Modulated Radiation Therapy (IMRT) that aims to deliver high radiation doses to the hypoxic areas, but lower radiation doses (leading to less side effects for the patients) to the other tumor regions. [23] Up to now, IMRT required methodologies to image differently oxygenated regions in tumors. Several approaches have been reported to achieve this, however none of those is fully conclusive [23,24]. Our MMR-targeted STRIT approach circumvents the need for hypoxia imaging by directly attaching the therapeutic radionuclide to a Nb that targets hypoxic TAMs. One day after the last α-MMR STRIT treatment, enhanced levels of apoptosis were noticed in the ^{177}Lu-DTPA-anti-MMR treated tumors, suggesting that the efficacy of treatment may at least partly depend on the lethal radiation of cancer cells in the vicinity of the MMR^{hi} TAMs.

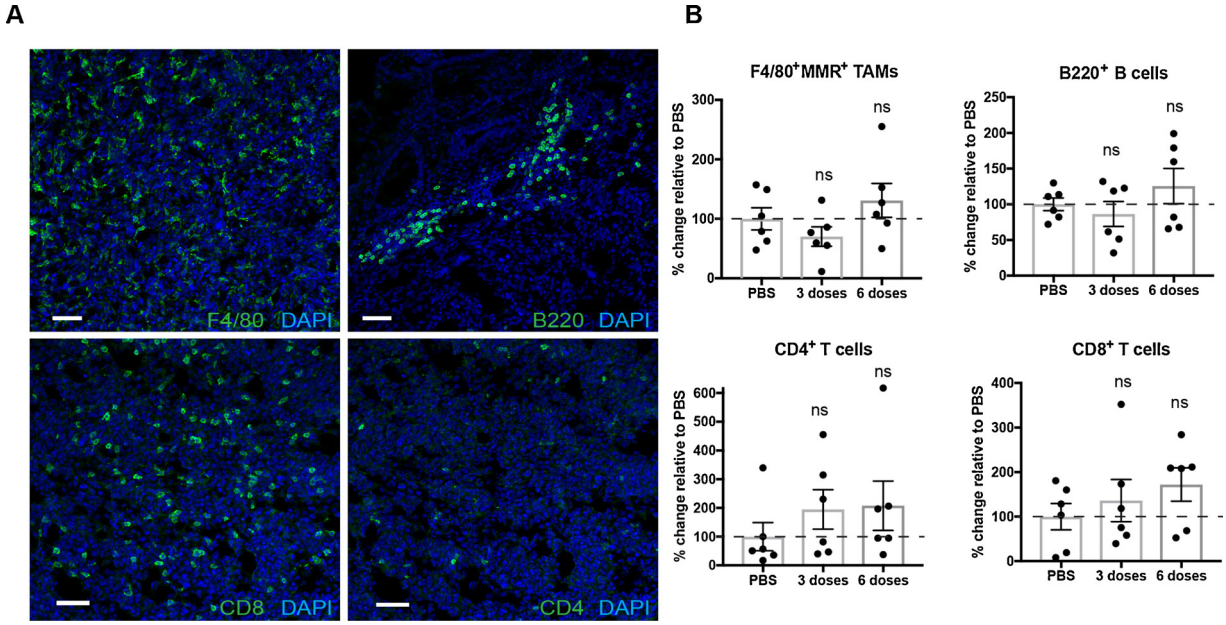

Fig. 7. MMR-targeted STRIT does not affect the immune infiltrate in late-stage tumors. A) TS/A tumors from mice treated with either three or six doses of ^{177}Lu-labeled α-MMR Nb or saline were removed at day 25 (two weeks after the last STRIT treatment) and stained for F4/80, MMR, B220, CD4, CD8 (Table S1, n = 6). Images of saline-treated (control) tumors are shown. Scalebar: 50 µm, B) Quantification of F4/80$^+$MMR$^+$ TAMs, B220$^+$ B cells, CD4$^+$ and CD8$^+$ T cells (n = 6).

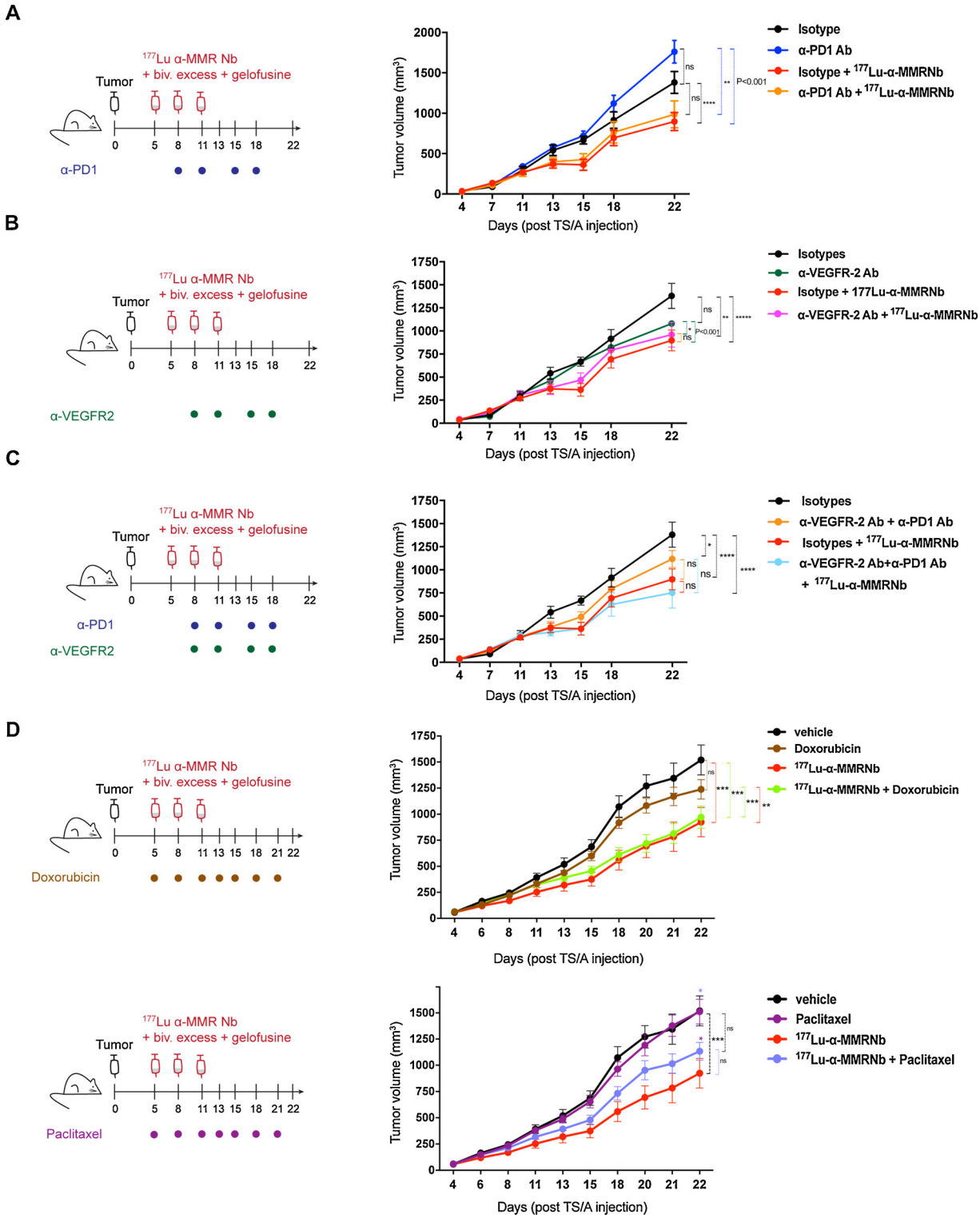

Fig. 8. MMR-targeted STRIT outcompetes the efficacy of currently used therapies. ^{177}Lu-labeled α-MMR Nb-mediated STRIT, either alone or in combination with A) intraperitoneal injections of α-mouse PD-1 mAb (RMP1-14, BioXCell) at 10 mg/kg of body weight (n = 8); B) identical conditions of α-mouse VEGFR-2 mAb (DC101, BioXCell) (n = 8); C) a combination of both α-mouse PD-1 and VEGFR-2 mAbs (n = 8) at the indicated schedules and D) doxorubicin (i.p., 2.5 mg/kg) or paclitaxel (i.v., 10 mg/kg) (n = 7–8). Tumor volume data were analyzed as repeated measurements (Genstat v19) and pairwise comparisons of the entire growth curves was done by a F-test; Student's *t*-test was performed to compare vehicle or paclitaxel-treated groups to group treated with combination of paclitaxel and STRIT at day 22 of tumor growth. The statistical significance in the figures is indicated as follows: *: $p < 0.05$; **: $p < 0.01$; ***: $p < 0.001$.

The extent at which immune cells are affected shortly after STRIT treatment needs further investigation. However, the immune cell compartment of STRIT-treated tumors, including TAMs, is fully restored at later stages of tumor growth (2 weeks after the last STRIT treatment), arguing against a permanent remodeling of the tumor immune compartment.

Since MMR is not uniquely expressed on TAMs, we optimized a strategy to block the extra-tumoral MMR antigenic sink, by co-injecting

a 100-fold molar excess of bivalent α-MMR Nb, to avoid therapy-induced toxicity. This strategy also limited toxicity related to kidney retention, an important aspect in TRNT as kidneys were reported to be the dose-limiting organ of radionuclide therapies targeting cancer cells, [4,6,7] as well as of our therapeutic α-MMR Nb. The need to avoid extra-tumoral antigen sinks has also been demonstrated for the Ab-mediated blockade of therapeutic targets such as CD47 [25] and Neuropilin-1 [26], suggesting that our strategy could have a broader applicability. The efficiency of bivalent Nbs for blocking extra-tumoral binding sites is due to a combination of increased avidity for the target (providing a competitive advantage to bivalent Nbs for rapidly occupying the target protein) and a larger size that reduces tumor penetrance. [10] Overall, we provide the first demonstration of a radioimmunotherapy targeting a tumor stromal cell, with clear therapeutic benefit against murine tumors that resist various standard-of-care therapies. Though clearly promising in a preclinical setting, from a clinical point of view STRIT needs further optimization to make sure that the dose delivered to kidney remains below an acceptable threshold level, while the dose delivered to tumors should be further maximized.

4. Materials and methods

4.1. Mice, cell line

Animal studies followed the guidelines of the institutional review board. Female Balb/c were from Janvier. The Balb/c mammary adenocarcinoma TS/A was inoculated subcutaneously in the right flank or orthotopically in the mammary fat pad (3×10^6 cells). Tumor volumes were calculated using the formula (D*d*d)*π/6, where D corresponds to the major tumor axis and d to the minor tumor axis.

4.2. Production and purification of monovalent and bivalent α-MMR Nb cl1

DNA fragments encoding for monovalent and bivalent α-MMR Nb cl1 were recloned in *Escherichia coli* expression vectors pHEN21 and pHEN6, that encode for untagged or hexahistidine-tagged variants, respectively. A nontargeting control Nb R3B23 [5] was produced similarly. The expression and production of Nbs was performed as previously described.10

4.3. Preparation of ^{111}In- and ^{177}Lu-DTPA conjugates

Untagged Nbs were reconstituted in sodium carbonate buffer (0.05 mol/L, pH 8.5) and conjugated with CHX-A"-DTPA [6]. Nb-DTPA conjugates were purified via SEC on Superdex Peptide 10/300 (GE Healthcare). The mean degree of DTPA conjugation per Nb was determined by ESI-Q-ToF-MS (Waters). $^{111}InCl_3$ was purchased from Curium with a specific activity of 1850 GBq/mg. Carrier-free $^{177}LuCl_3$ was obtained from ITG (Garching) with a specific activity of 3000 GBq/mg. The desired activity of ^{111}In (37–185 MBq) or ^{177}Lu (37–1000 MBq) was added to a test vial containing ammonium acetate (0.2 mol/L, pH 5.0) and incubated with the Nb-DTPA conjugates (50–100 mg) for 30′ at 50 °C. Next, the mixtures were purified and reconstituted in 0.9% saline with 5 mg/ml ascorbic acid, using disposable NAP-5 gel filtration columns (GE Healthcare), and filtered through a 0.22-mm filter. Radiochemical purity (RCP) was evaluated using instant Thin Layer Chromatography (using 0.1 M sodium citrate as mobile phase) and radio-SEC using Superdex 75 5/15 column (GE Healthcare), with 0.01 mol/L PBS/0.3 mol/L NaCl solution used as mobile phase.

4.4. Ex vivo biodistribution of ^{111}In-labeled and ^{177}Lu-labeled Nb conjugates in mice bearing subcutaneous or orthotopic TS/A tumors

13-day-old subcutaneous TS/A-bearing mice were injected intravenously with ^{111}In-DTPA-monovalent α-MMR Nb or ^{111}In-DTPA-bivalent α-MMR Nb (see Results section for activity). Mice were sacrificed at different time points after injection (1 h, 3 h, 6 h, 24 h and 48 h) followed by the isolation of different organs, tissues and tumors. The radioactivity present in the different samples was measured against a standard of known radioactivity using a γ-counter and expressed as % IA per gram tissue (%IA/g), corrected for decay.

For the biodistribution of ^{177}Lu-labeled Nbs, ^{177}Lu-DTPA-monovalent α-MMR Nb with a 100-fold molar excess of unlabeled bivalent α-MMR Nb (see Results section for activity) and 150 mg/kg gelofusine was i.v. injected in 13-day s.c. TS/A tumor-bearing mice, which were euthanized at several time points up to 120 h, dissected and major organs and tissues were isolated, weighed, counted and expressed as %IA/g. Alternatively, mice with 13-day orthotopic TS/A tumors growing in the mammary fat pad were i.v. injected with either ^{177}Lu-DTPA-monovalent non-targeting R3B23 Nb or ^{177}Lu-DTPA-monovalent α-MMR Nb, alone and with a 100-fold molar excess of unlabeled bivalent α-MMR Nb (n = 3 per condition) + gelofusine. Mice were euthanized after 1 h and analysed as described above.

4.5. Blocking strategy with different fold excesses of bivalent α-MMR Nb

^{111}In-DTPA monovalent α-MMR Nb at an activity of 2.05 ± 0.17 MBq (1 μg Nb, RCP: 96%) was co-injected with a 20-, 50- or 100-fold molar excess of unlabeled bivalent α-MMR Nb in TS/A-bearing mice (13 days s.c. tumor growth). Organs/Tissues were dissected at 1 h, 6 h and 24 h p.i. and tracer uptake was expressed as %IA/g.

4.6. Biodistribution of ^{111}In-DTPA-monovalent α-MMR Nb via molecular imaging

TS/A tumor-bearing mice were i.v. injected in the tail vein with ^{111}In-labeled Nbs and gelofusine (see Results section for dosing) followed by micro-SPECT/CT imaging after 1 h. Mice were anaesthetized using 2% isoflurane and kept warm using a heating pad. Micro-SPECT/CT imaging was performed with a Vector$^+$/CT MILabs system, using a SPECT-collimator and a spiral scan mode of 6 bed positions (150 s per position). For CT, a normal scan mode of only one position was used. The obtained SPECT-data were reconstructed with a 0.4 voxel size, 2 subsets and 4 iterations, after which images were fused and corrected for attenuation based on the CT-scan. Images were analyzed using a medical image data analysis tool (AMIDE) and OsiriX. Uptake of ^{111}In-labeled Nb in organs and tissues was analyzed and expressed as % injected activity per cubic centimeter (%IA)/cm^3.

4.7. Organ-absorbed doses of ^{177}Lu-DTPA-monovalent α-MMR Nb

The long-term biodistribution data were time-integrated to obtain the residence time per gram tissue. Briefly, the area under the curve between 0 and 120 h was made using the trapezoid integration method. Next, the absorbed doses were calculated using S values for ^{177}Lu obtained from RADAR phantoms (Unit Density Spheres). The S value for a 1 g sphere (0.0000233 Gy.g/MBq.s) was used to calculate all organ doses.

4.8. Toxicity of ^{177}Lu-DTPA-monovalent α-MMR Nb

Two separate toxicity studies were performed: 1) naïve Balb/c mice were injected i.v. with (i) a single dose of ^{177}Lu-labeled α-MMR Nb together with a 100-fold molar excess of unlabeled bivalent α-MMR Nb and compared to (ii) mice that were injected with ^{177}Lu-labeled α-MMR Nb alone and (iii) control mice injected with 0.9% saline, after which survival was followed. 2) naïve Balb/c mice were injected intravenously with (i) three doses ^{177}Lu-labeled α-MMR Nb together with 100-fold molar excess of unlabeled bivalent α-MMR Nb and compared

to (ii) mice that were injected with ^{177}Lu-labeled α-MMR Nb alone and (iii) control mice injected with 0.9% saline. All mice were co-injected i.v. with 150 mg/kg gelofusine. Nb activities are provided in the Results section. Parameters evaluated were clinical signs, mortality, changes in body weight, food intake and histopathology of organs. The kidneys, liver and spleen of treated mice were sampled, formalin-fixed and sent to AnaPath Services GmbH (Liestal, Switzerland) where they were trimmed, processed, and embedded in paraffin wax. 4 μm sections were taken, stained by hematoxylin and eosin and examined by light microscopy. Several histopathological parameters (HP) were measured (Supplementary Materials and Methods and Table 1). Serum was analyzed for alanine aminotransferase (ALT kit; Sigma-Aldrich), indicative of liver toxicity.

4.9. Micro-autoradiography

Frozen sections of 10 μm thickness were mounted on Superfrost slides, air-dried and fixed in 4% PFA for 10 min at room temperature, washed three times in PBS and dehydrated in graded ethanol (30, 50, 70%) after which they were air-dried prior micro-autoradiography (MAR). MAR was performed in complete darkness by using ILFORD K2 nuclear photographic emulsion. Following dipping the slides into the emulsion, excess emulsion was drained off and the slides were air-dried for 10 min and incubated at 4 °C for 4 days (exposure time). Following exposure, the slides were incubated for 30 min at room temperature after which they were photographically processed (developing steps in dark room: 1) Kodak D19 developer (Kodak-Pathé #5,027,065) for 7 min, 2) 4% acetic acid for 15 s, 3) Ilford Hypam rapid fix (#758,285) for 10 min, 4) 2x water for 15 s), counter-stained with Harris Hematoxylin stain and cover-slipped for analysis.

4.10. Immunohistochemistry

For hypoxia staining, tumor-bearing mice were injected with 80 mg/kg body weight pimonidazole (Hypoxyprobe-1, HP-1, HPI Inc.) and 2 h later tumors were collected. Tumors were fixed in 4% paraformaldehyde (PFA), snap frozen, sections of 12 μm were obtained in cryostat and stained for F4/80, MMR, CD19, CD4, CD8, HP-1, cleaved caspase-3 (Table S1) and 4′, 6-diamidino-2-phenylindole (DAPI). Slides were imaged with an Axio Scan.Z1 microscope (Zeiss, Germany). Images were acquired with either a 10X Plan-Apochromat 0.45 NA or a 20X Plan-Apochromat 0.8 NA dry objectives, using a Hamamatsu Orca Flash camera. Images were analyzed with Zen (blue edition). Quantification of F4/80$^+$MMR$^+$ TAMs, B220$^+$ B cells, CD4$^+$ T cells, CD8$^+$ T cells and cleaved caspase-3$^+$ cells was performed in QuPath software (version 0.1.2).

4.11. Statistical analyses

Tumor volumes were analyzed as longitudinal data (repeated measurements over time) using the residual maximum likelihood (REML) as implemented in Genstat v19 [27] (Supplementary Information). All other statistical analyses were performed using Students' *t* test (GraphPad Prism Software). Statistical significance is indicated as follows: *: $p < 0.05$; **: $p < 0.01$; ***: $p < 0.001$.

Financial support

This work was supported by a doctoral grant from IWT-Vlaanderen to E.B.; an Innoviris Attract – Brains for Brussels grant to K.M.; a grant from "Kom op tegen Kanker", "Stichting tegen Kanker" and Research Foundation Flanders (FWO) to J.A.V.G.; a grant from "Kom op tegen Kanker" to G.R., K.M. and N.D.; a VUB-IOF and VUB-Strategic Research Program (SRP) to T.L. and J.A.V.G.; a FWO-SBO grant to J.A.V.G, G.R., N.D. and T.L. M.D. is a postdoctoral researcher of FWO. J.A.V.G. and K.M. are members of the EU − COST action Mye-EUNITER. The funding sources had no involvement in the study design.

Declaration of Competing Interest

T.L., G.R., N.D., K.M. and J.A.V.G. hold patents on α-MMR imaging and therapy. T.L., G.R., N.D. and M.D. are co-founders and employees/consultants for the company CAMEL-IDS that focuses on nanobody-based radionuclide therapy. The other authors have no conflicting financial interests.

CRediT authorship contribution statement

Evangelia Bolli: Conceptualization, Data curation, Formal analysis, Investigation, Methodology, Visualization, Writing - original draft. **Matthias D'Huyvetter:** Conceptualization, Data curation, Formal analysis, Investigation, Methodology, Visualization, Writing - review & editing. **Tony Lahoutte:** Conceptualization, Funding acquisition, Resources, Supervision. **Amanda Gonçalves:** Data curation, Formal analysis, Funding acquisition, Investigation, Methodology. **Marnik Vuylsteke:** Formal analysis, Software. **Geert Raes:** Conceptualization, Funding acquisition, Writing - review & editing. **Nick Devoogdt:** Conceptualization, Funding acquisition, Methodology, Project administration, Resources, Supervision, Writing - review & editing. **Kiavash Movahedi:** Conceptualization, Data curation, Formal analysis, Methodology, Supervision, Visualization, Writing - review & editing. **Jo A. Van Ginderachter:** Conceptualization, Funding acquisition, Methodology, Project administration, Resources, Supervision, Writing - review & editing.

Acknowledgments

The authors wish to thank Ella Omasta, Marie-Thérèse Detobel, Cindy Peleman, Claudia Mebis, Jan De Jonge, Maria Slazak and Nadia Abou for technical and administrative assistance. Massimiliano Mazzone (VIB, KULeuven) is thanked for providing doxorubicin and paclitaxel.

Appendix A. Supplementary data

Supplementary material related to this article can be found, in the online version, at doi:https://doi.org/10.1016/j.jconrel.2019.10.024.

References

[1] M.J. Lambert, A. Berkenblit, Antibody–drug conjugates for cancer treatment, Annu. Rev. Med. 69 (2018) 191–207.
[2] M.D. Bartholomä, Radioimmunotherapy of solid tumors: approaches on the verge of clinical application, J. Label Compd. Radiopharm. 61 (2018) 715–726.
[3] S.M. Larson, J.A. Carrasquillo, N.K. Cheung, O.W. Press, Radioimmunotherapy of human tumours, Nat. Rev. Cancer 15 (2015) 347–360.
[4] M. D'Huyvetter, C. Xavier, V. Caveliers, T. Lahoutte, S. Muyldermans, N. Devoogdt, Radiolabeled nanobodies as theranostic tools in targeted radionuclide therapy of cancer, Expert Opin. Drug Deliv. 11 (2014) 1939–1954.
[5] M. Lemaire, M. D'Huyvetter, T. Lahoutte, E. Van Valckenborgh, E. Menu, E. De Bruyne, et al., Imaging and radioimmunotherapy of multiple myeloma with anti-idiotypic Nanobodies, Leukemia 28 (2014) 444–447.
[6] M. D'Huyvetter, J. De Vos, C. Xavier, M. Pruszynski, Y.G.J. Sterckx, S. Massa, et al., ^{131}I-labelled A-HER2 camelid sdAb as a theranostic tool in Cancer treatment, Clin. Cancer Res. 23 (2017) 6616–6628.
[7] A. Krasniqi, M. D'Huyvetter, C. Xavier, K. Van der Jeught, S. Muyldermans, J. Van Der Heyden, et al., Theranostic radiolabelled A-CD20 sdAb for targeted radionuclide therapy of non-hodgkin lymphoma, Mol. Cancer Ther. 16 (2017) 2828–2840.
[8] E. Bolli, K. Movahedi, D. Laoui, J.A. Van Ginderachter, Novel insights in the regulation and function of macrophages in the tumor microenvironment, Curr. Opin. Oncol. 29 (2017) 55–61.
[9] K. Movahedi, D. Laoui, C. Gysemans, M. Baeten, G. Stangé, J. Van den Bossche, et al., Different tumor microenvironments contain functionally distinct subsets of macrophages derived from Ly6C(high) monocytes, Cancer Res. 70 (2010) 5728–5737.
[10] K. Movahedi, S. Schoonooghe, D. Laoui, I. Houbracken, W. Waelput, K. Breckpot, et al., Nanobody-based targeting of the macrophage mannose receptor for effective

in vivo imaging of tumor-associated macrophages, Cancer Res. 72 (2012) 4165–4177.
[11] A. Blykers, S. Schoonooghe, C. Xavier, K. D'hoe, D. Laoui, M. D'Huyvetter, et al., PET imaging of macrophage mannose receptor-expressing macrophages in tumor stroma using 18F-Radiolabelled camelid single-domain antibody fragments, J. Nucl. Med. 56 (2015) 1265–1271.
[12] H.E. Barker, J.T.E. Paget, A.A. Khan, K.J. Harrington, The tumour microenvironment after radiotherapy: mechanisms of resistance and recurrence, Nat. Rev. Cancer 15 (2015) 409–425.
[13] M. D'Huyvetter, C. Vincke, C. Xavier, A. Aerts, N. Impens, S. Baatout, et al., Targeted radionuclide therapy with A 177Lu-labeled anti-HER2 nanobody, Theranostics 4 (2014) 708–720.
[14] P. Sharma, S. Hu-Lieskovan, J.A. Wargo, A. Ribas, Primary, adaptive, and acquired resistance to cancer immunotherapy, Cell 168 (2017) 707–723.
[15] Y. Itatani, K. Kawada, T. Yamamoto, Y. Sakai, Resistance to anti-angiogenic therapy in cancer-alterations to anti-VEGF pathway, Int. J. Mol. Sci. 19 (2018) 1–18.
[16] L. Wein, S. Loi, Mechanisms of resistance of chemotherapy in early-stage triple negative breast cancer (TNBC), Breast 34 (2017) S27–S30.
[17] J.M. Brown, The hypoxic cell: a target for selective cancer therapy. Eighteenth Bruce F. cain memorial award lecture, Cancer Res. 59 (1999) 5863–5870.
[18] I. Dagogo-Jack, A.T. Shaw, Tumour heterogeneity and resistance to cancer therapies, Nat. Rev. Clin. Oncol. 15 (2018) 81–94.
[19] K. Movahedi, J.A. Van Ginderachter, The ontogeny and microenvironmental regulation of tumor-associated macrophages, Antioxid. Redox Signal. 25 (14) (2016) 775–791.
[20] E. Van Overmeire, B. Stijlemans, F. Heymann, J. Keirsse, Y. Morias, Y. Elkrim, et al., M-CSF and GM-CSF receptor signaling differentially regulate monocyte maturation and macrophage polarization in the tumor microenvironment, Cancer Res. 76 (1) (2016) 35–42.
[21] D. Laoui, E. Van Overmeire, G. Di Conza, C. Aldeni, J. Keirsse, Y. Morias, et al., Tumor hypoxia does not drive differentiation of tumor-associated macrophages but rather fine-tunes the M2-like macrophage population, Cancer Res. 74 (2014) 24–30.
[22] A. Casazza, D. Laoui, M. Wenes, S. Rizzolio, N. Bassani, M. Mambretti, et al., Impeding macrophage entry into hypoxic tumor areas by Sema3A/Nrp1 signaling blockade inhibits angiogenesis and restores antitumor immunity, Cancer Cell 24 (6) (2013) 695–709.
[23] F. Colliez, B. Gallez, B.F. Jordan, Assessing tumor oxygenation for predicting outcome in radiation oncology: a review of studies correlating tumor hypoxic status and outcome in the preclinical and clinical settings, Front. Oncol. 7 (2017) 10, https://doi.org/10.3389/fonc.2017.00010.
[24] D.R. Grimes, D.R. Warren, S. Warren, Hypoxia imaging and radiotherapy: bridging the resolution gap, Proc. Natl. Acad. Sci. U. S. A. 114 (2017) 10184–10189.
[25] J.R. Ingram, O.S. Blomberg, J.T. Sockolosky, L. Ali, F.I. Schmidt, N. Pishesha, et al., Localized CD47 blockade enhances immunotherapy for murine melanoma, Proc. Natl. Acad. Sci. U. S. A. 114 (2017) 10184–10189.
[26] D. Bumbaca, H. Xiang, C.A. Boswell, R.E. Port, S.L. Stainton, E.E. Mundo, et al., Maximizing tumour exposure to anti-neuropilin-1 antibody requires saturation of non-tumour tissue antigenic sinks in mice, Br. J. Pharmacol. 166 (1) (2012) 368–377.
[27] D. Baird, D. Murray, R. Payne, D. Soutar, An Introduction to GenStat for Windows, 19th edition, VSN International, 2018.